공학석사학위논문

Performance Analysis of Lidar-based Lunar Landing Point Designation and its Verification Using Quadrotor

라이다기반 달 착륙지 선정기법 성능분석 및 쿼드로터를 이용한 성능검증

2016 년 2 월

서울대학교 대학원

기계항공공학부

이 충 민

Abstract

Performance Analysis of Lidar-based Lunar Landing Point Designation and its Verification Using Quadrotor

LEE, CHOONG MIN

DEPARTMENT OF MECHNICAL AND

AEROSPACE ENGINEERING

COLLEGE OF ENGINEERING

SEOUL NATIONAL UNIVERSITY

A Lidar-based safe landing technique fundamentally estimates the slope and roughness of lunar terrain using three-dimensional range measurement, and designates the landing target that terrain parameters have the minimum value. In the case of hazard cost calculation only with the parameters, however, the selected target can be located near hazards on the surface such as craters, rocks and slants which are able to

damage lunar lander. Therefore, relative distance to hazard should also be considered simultaneously in order to choose the landing point which is not only gentle but also as far from hazard as possible. In this case, the effect of terrain condition on the safe landing performance should be closely analyzed since it is influenced by the level of the terrain parameters. In this thesis, the relation between terrain condition and the performance of landing site designation with the relative distance to hazard was analyzed, and it was confirmed that the best landing target can be selected by the weighted sum of the parameters and relative distance to hazard reflecting the terrain characteristics of landing area through simulations and experiments with a quadrotor with TOF camera.

Keywords: Hazard Detection and Avoidance(HDA), Light detection and ranging(Lidar), Depth camera, TOF camera, Quadrotor

Student Number: 2014-20663

Contents

List of Figures

List of Tables

Chapter 1

Introduction

1.1 Motivation and Background

A precise and accurate navigation technique is necessary for the safe landing of lunar lander. The Autonomous Landing and Hazard Avoidance technology (ALHAT) project of NASA specifically aims the landing precision into 90m (3-σ), and the

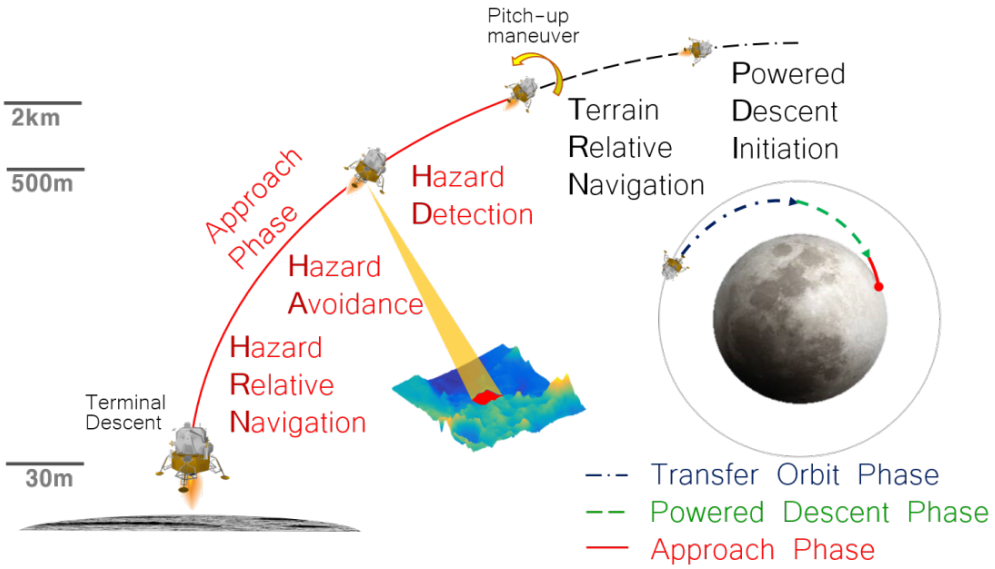

Figure 1.1 ALHAT mission profile of lunar landing

research about Hazard Detection and Avoidance (HDA) technique which is one of essential technique to meet the requirement and to succeed safe lading has been conducted[1].

The ALHAT Mission profile of lunar landing according to height above ground is shown in Figure 1.1. The lunar lander leaves the lunar orbit of 100km high and begins Powered Descent Initiation (PDI) phase where it starts breaking with reverse thrust. From the 15kms high, it starts Terrain Relative Navigation (TRN) in order to update current position. From the 2kms high, HDA system detects various hazards on the lunar surface such as craters, rocks, and slants. Finally, it lands on the best landing target designated by HDA system using the hazard information.

The lunar landers of Apollo mission were likely to land on areas near the equator where few hazard existed and the lighting condition was ideal. The landings were manually performed by the crew viewing out and identifying hazards. In the case of Apollo 15, it landed near the rim of a shadowed crater and one of its footpad was entered it. This caused 11° tilt angle of attitude at the moment of touch down and finally resulted in damage of main engine bell. Thus, an advanced safe landing technology has been necessary for the safe lunar landing[2].

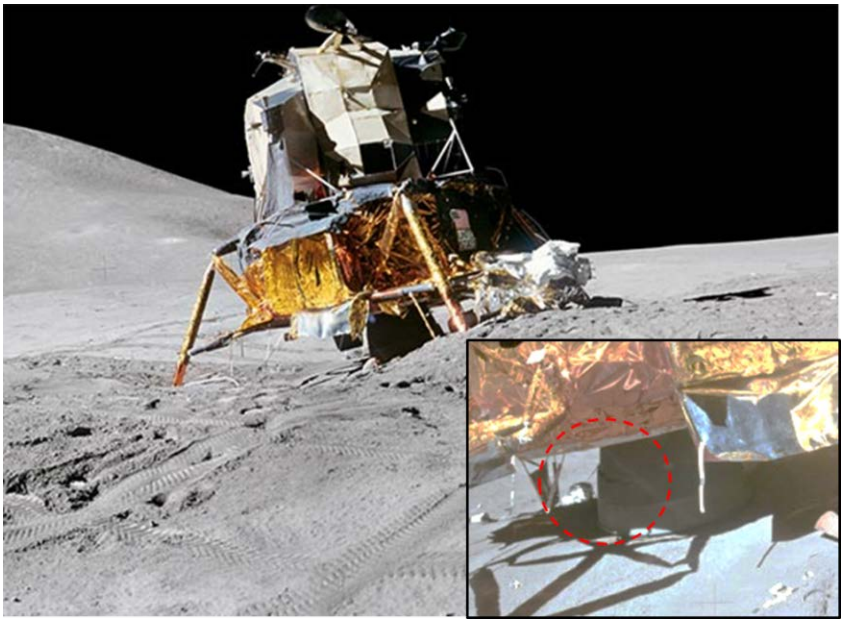

Figure 1.2 Apollo 15 landed on the lunar surface and damage on main engine skirt

Recent research of the NASA's Constellation program lays out the lunar landing mission not only for the safe landing on the naïve lunar surface but especially on the veiled places where presence of water ice is expected and plentiful resources exist such as polar area. The area has harsh condition with a wide variety of hazards. By developing robust HDA system, however, a technical basis for landing on the hazardous places can be obtained. In order to guarantee safe landing on the severe lunar surface, the lander should precisely and accurately detect and avoid the hazards.

For this work, a huge data with respect to topological features of lunar surface has

been acquired from Lunar Reconnaissance Orbiter (LRO) equipped with Lunar Orbiter Laser Altimeter (LOLA) which provides a precise global topological model and geodetic grid. However, it is difficult to precisely detect and avoid small hazards with it since resolution the database is not high enough even if they are still big enough to damage the lander. Thus, It is very important to precisely detect and avoid them in advance[3].

There are a wide verity sensors for the HDA like Radar, camera and light detection and ranging (Lidar) sensor. The radar provides very long-range measurement compared to other range sensor, but it has low precision and resolution[4]. The research about the HDA technique based on optical camera image has been actively conducted because it is light, low price. This identifies hazards on the lunar surface using various image processing techniques. It detects rocks and craters by ellipse fitting to the hazards[5]. Stereovision is also used for the HDA. It directly provides the three-dimensional range measurement by computing binocular images. However, the quality of a camera image is very sensitive to external light condition which is closely related to sun incidence angle on the moon. The landers of next lunar projects in the future aim to land on harsh area where water ice and numerous resources are expected to exist in the arctic region. These areas are normally rugged and sparsely lighted. Thus, in the ALHAT project, the

HDA based on Lidar which measure three dimensional range with very high speed regardless of any light condition.

The Lidar is a promising range sensor providing three-dimensional distance measurement by emitting laser and measuring its time of flight regardless of any light condition While the resolution of radar is low and camera is sensitive to light condition. The HDA technique based on Lidar basically estimates two terrain parameters: the slope and roughness which are one of the most representative characteristics of terrain[6]. They are estimated from a smooth plane which is calculated by approximating Lidar measurement to a plane as big as the lander's footprint and used to calculate hazard cost map that the bigger parameters are, the bigger hazard cost is. Finally, the point with the smallest hazard cost is selected as the best safe landing target. In this case, the target can be located near the hazards because of the terrain condition and they can damage the lander. In order to solve this problem, hazard cost based on relative distance to hazards which has cost inversely proportional to the distance is applied and integrated the terrain parameters[7][8]. Therefore, an optimal landing point free of hazard can be designated with the integrated hazard cost map. Previous works about the Lidar-based HDA technique did adopt the Distance To the Nearest Hazard (DTNH) and analyze hazard detection performance especially relating to roughness.

However, the researches did not closely look into the relation between the slants which are the area with hazard cost exceeding the maximum tolerance and the HDA performance yet.

1.2 Objectives and Contributions

In the previous research according to the Lidar-based HDA technique applied hazard cost based on distance to hazards in order to improve the performance of landing point designation. However, any specific method of the application was not clearly dealt with and the relation between the integration technique and topological aspects was not analyzed in detail. This thesis emphasizes that hazard cost according to both the slope and roughness-based distance should be simultaneously considered and integrated with the cost of the two terrain parameters based on adaptive weighting strategy. The effect of the cost maps based on relative distance to both rocks and slants on the performance of hazard avoidance is analyzed with respect to the characteristics of the terrain the improved performance is shown as grounds of the assertion. A quadrotor drone which is automatically controlled based on VICON motion capture system and a TOF camera that is short-range flash Lidar for indoor is utilized to confirm the feasibility of the proposed HDA technique.

1.3 Organization

This thesis is organized as follows: lunar terrain parameter estimation, landing site designation and hazard cost based on relative distance to hazard in chapter 2. In chapter 3 and 4, the HDA results from various combinations of the parameters and distance-based hazard cost are compared to each other and analyzed by simulation and experiment, and this is concluded in chapter 5.

Chapter 2

Hazard Detection and Avoidance Landing

2.1 Introduction

The HDA systems acquire the terrain information using various HDA sensors. Especially, Lidar-based HDA system finds the safest landing point using terrain parameters; the slope and roughness calculated by the three-dimensional range measurement from Lidar. The parameters are estimated from smooth planes which are

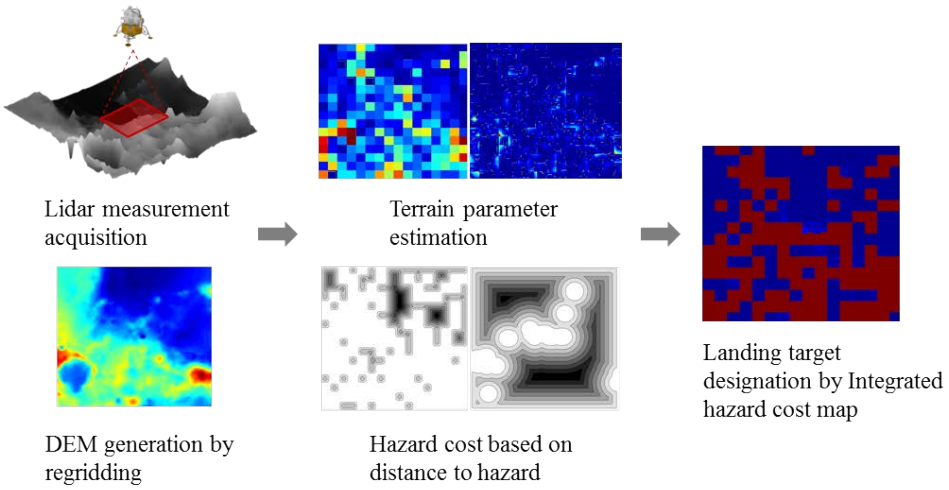

Figure 2.1 HDA processing steps

the approximation of terrain's Digital Elevation Model (DEM) based on Least Median Square(LMedS) method.

The points or area with bigger terrain parameters than the maximum tolerance of them are determined as hazards. The HDA system chooses the best landing site having the minimum cost avoiding them. The HDA process is illustrated in Figure 2.1. The selected landing point can be located near the detected hazard if it just looks for the point with small slope and roughness even the range measure can worsen this circumstance. However, hazard cost map based on relative distance to the nearest hazards should be considered with the parameters simultaneously in order to choose the landing point not only with small hazard cost but also as far from the hazards as possible.

2.2 Uniform DEM generation

Since the lunar terrain has complicated topographical features like rocks, slopes and craters, Lidar measures three-dimensional range on irregular horizontal points. In order to improve the efficiency of data processing, the Digital Elevation Model (DEM) is generated by mapping the measurement on a uniform grid[6][9]. When the Lidar is located on Cartesian coordinate above the ground and measures the range in vertical

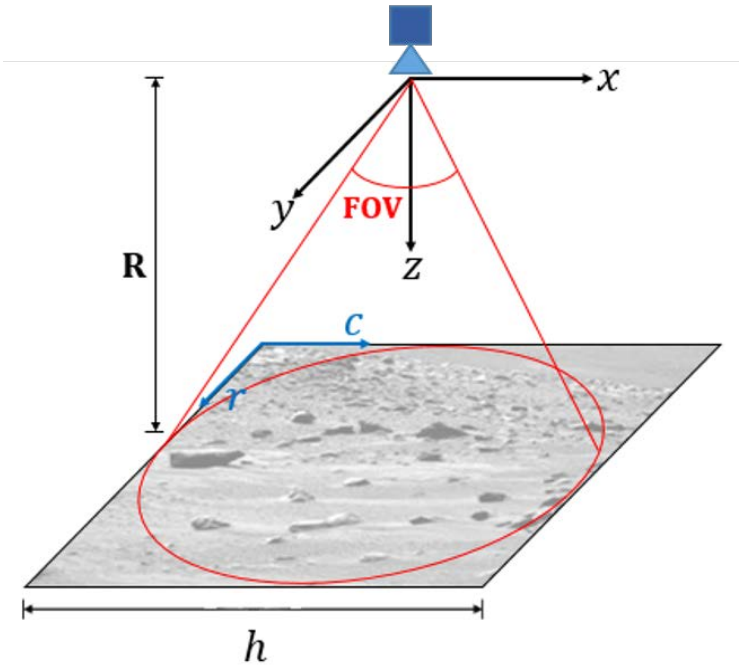

Figure 2.2 Lidar coordinate

$$s = h / n,\ \ h = 2L\tan(f\ / 2) \tag{1}$$

$$(r,\ c) = (y / s + n / 2,\ x / s + n / 2) \tag{2}$$

direction as shown in Figure 2.2. Ground Sample Distance (GSD) *s* which is the unit of the grid coordinate is calculated to convert Lidar coordinate to *r*, *c* grid coordinate by the number of sample *n*, horizontal distance of the map h and mean distance *L*.

With the grid coordinate, DEM can be generated by bilinear interpolation which is simple expansion of one-dimensional interpolation to two-dimension[10]. For instance, the weights of data on the grid nodes surrounding the measurement z_1 shown in Figure 2.3 are calculated as follows.

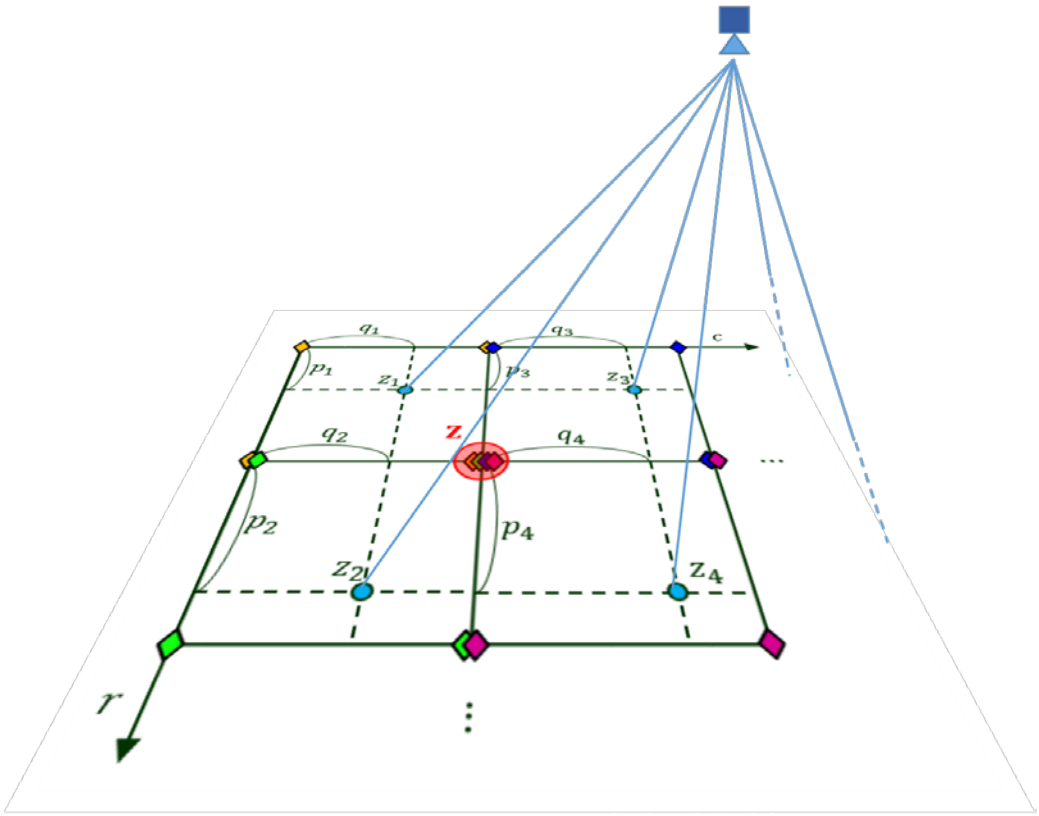

Figure 2.3 Regridding based on bilinear interpolation

$$
\begin{aligned}
&p_1 = r - \lfloor r \rfloor, \quad q_1 = c - \lfloor c \rfloor \\
&E(r,c) \mathrel{+}= (1-p_1)(1-q_1)\, z_n \\
&E(r+1,c) \mathrel{+}= p_1(1-q_1)\, z_n \\
&E(r,c+1) \mathrel{+}= (1-p_1)q_1\, z_n \\
&E(r+1,c+1) \mathrel{+}= p_1 q_1\, z_n
\end{aligned}
\tag{3}
$$

Likewise, the weights from z_2, z_3 and z_4 are calculated. Accordingly, the elevation on the grid node surrounded by the four measurements can be estimated by normalizing the accumulated elevation data with respect to the node *Z*.

$$
\begin{aligned}
E &= p_1 q_1 z_1 + (1-p_2) q_2 z_2 \\
&\quad + p_3 (1-q_3) z_3 + (1-p_4)(1-q_4) z_4 \\
W &= p_1 q_1 + (1-p_2) q_2 \\
&\quad + p_3 (1-q_3) + (1-p_4)(1-q_4) \\
Z(r,c) &= E(r,c) / W(r,c)
\end{aligned}
\tag{4}
$$

2.3 Lunar Terrain Parameter Estimation

2.3.1 Slope and Roughness

A wide variety of topological features with craters rocks, and cliffs on the lunar surface. The slope and roughness are useful terrain parameters to express the characteristics of lunar terrain. The slope is the angle between current gravity vector of the lander and the normal vector of an approximated unit surface called ‘smooth plane’.

2.3.2 Terrain Approximation

In order to estimate the slope and roughness, complex terrain of desired landing area is approximated to planes which is call ‘smooth planes’. LMedS method is applied to calculate them. Because median is rarely influenced by outliers of data in contrast to mean used in least square method, a specific area can be nicely approximated into a simple plane in the case of outlier distribution below 50%[11]. In this case, LMedS approximation algorithm should be especially designed suitable for a specific system

rather than derived to closed form like least square since median is determined by the order of data regardless of size itself. The plane fitting algorithm based on LMedS is discussed below.

First of all, because at least three points are necessary to determine of a plane, a small part of area as big as the lander's footprint is assigned, and three points ($\mathbf{x}_a$, $\mathbf{x}_b$, $\mathbf{x}_c$) are randomly selected among the elevation data in the part. The plane equation from the selected points is derived

$$\mathbf{n} \cdot \mathbf{x} + d = \mathbf{0} \tag{5}$$

$$\mathbf{n} = (\mathbf{x_b} - \mathbf{x_a}) \times (\mathbf{x_c} - \mathbf{x_a}), \quad d = -\mathbf{n} \cdot \mathbf{x_a} \tag{6}$$

and square plane errors r_i are calculated with respect to the rest points x_i.

$$\{r_i\} = \left\{ (\mathbf{n} \cdot \mathbf{x}_i + d)^2 \right\} \tag{7}$$

The median of the square plane errors is saved, and the best plane parameters $\mathbf{n}_{best}$, d_{best} are acquired as a result of iteration of this algorithm. In this case, the iteration number t is determined the probability o of outlier(rock) distribution and the probability P that least a triple is selected without any outlier.

$$P = 1-(1-(1-o)^3)^t, \;\; t = \left\lceil \frac{\ln(1-P)}{\ln\left\{1-(1-o)^3\right\}} \right\rceil \tag{8}$$

Once the best plane parameters are determined, robust standard deviation is calculated according to square plane errors from cumulative probability distribution function where the r_{median} is median value of the square plane errors on a plane.

$$\sigma_r = 1.4826\left\{1+\left(\frac{5}{t-3}\right)\right\} r_{median} \tag{9}[12]$$

The outliers satisfying the inequality are eliminated and the smooth plane can be acquired by standard least square plane fitting only with inliers.

$$r_i = (\mathbf{n}_{best} \cdot \mathbf{x}_i + d_{best})^2 > \sigma_r \tag{10}$$

Figure 2.4 briefly accounts for the entire plane approximation algorithm. The slope **A** and roughness **R** can be estimated using the surface normal **n** of the approximated plane and elevation z_s of the smooth plane where $\mathbf{n}_g$ is the local gravity vector of the lander.

$$z_s = -(n_x x + n_y y + d)/n_z,\ \mathbf{n} = \left[n_x,\ n_y,\ n_z \right] \tag{11}$$

$$\mathbf{A}(r,c) = \cos^{-1}(\mathbf{n} \cdot \mathbf{n}_g / \| \mathbf{n} \| \| \mathbf{n}_g \|) \tag{12}$$

$$\mathbf{R}(r,c) = | \mathbf{Z}(r,c) - \mathbf{Z}_s(r,c) | \tag{13}$$

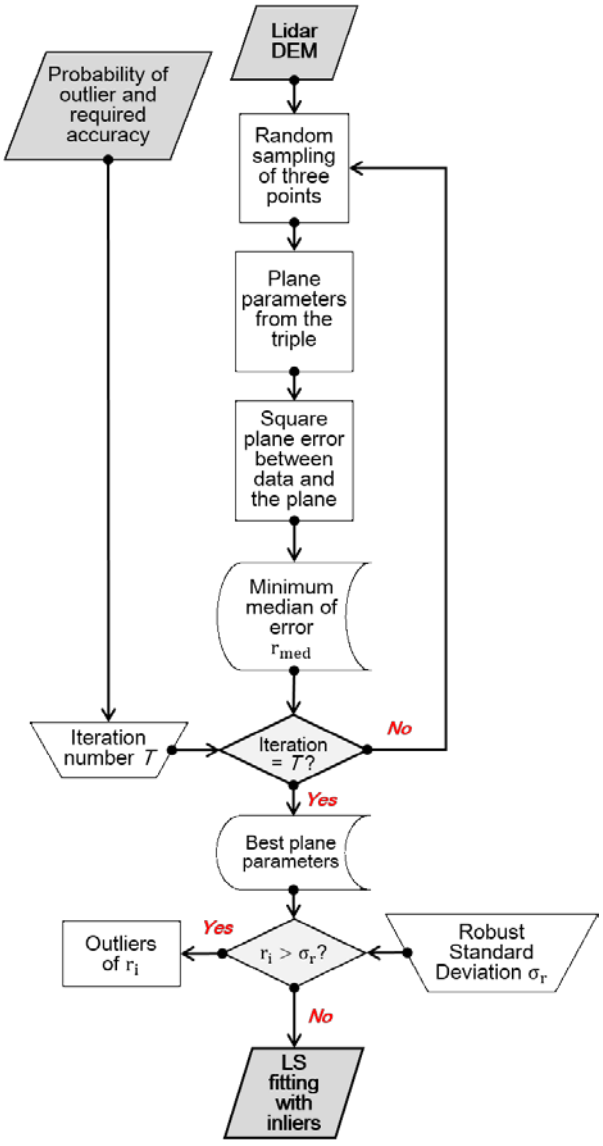

Figure 2.4 Flow chart of the plane fitting algorithm based on least median square

2.4 Hazard Cost Based on Lunar Terrain Parameters

A hazard cost is calculated by multiplying the slope and roughness from the smooth plane and normalizing it using hazard tolerances A_{THR}, R_{THR} which are related to the two terrain parameters respectively and determined by the ALHAT Landing precision requirement[6]. The hazard cost map consists of the cost on the grid coordinate.

$$\mathbf{C}(r,c)=\begin{cases} 1 & \mathbf{A}(r,c) > A_{THR} \\ & , \ or \ \mathbf{R}(r,c) > R_{THR} \\ \dfrac{\left[\mathbf{R}(r,c)\times\mathbf{A}(r,c)\right]}{R_{THR}\times A_{THR}} & , \text{ otherwise} \end{cases} \tag{14}$$

The point of the minimum cost is the safest point and can be selected the best landing point. However, it can be located near hazards since only the cost value was considered, this does not guarantees safe landing. Thus, safe landing point as far from hazard as possible can be designated by considering distance to hazards.

2.5 Hazard Cost Based on Relative Distance to Hazard

Points with the cost exceeding the slope and roughness tolerance are defined as slant and rock respectively. These points are determined as hazards and hazard cost map that

cost is inversely proportional to distance to the nearest hazard is obtained[8]. As shown in Figure 2.5, arbitrary point P_1 and the shortest distance I_1 from P_1 to the nearest hazard. Likewise, I_2, I_3 with respect to P_2, P_3 can be acquired. Generalized distance to the nearest hazard can be expressed with n hazards as

$$I_i = \left| P_i - P_{hazard_j} \right|, \quad j = 1, 2, \cdots, n \tag{15}$$

Next, hazard cost inversely proportional to distance I is calculated and normalized with

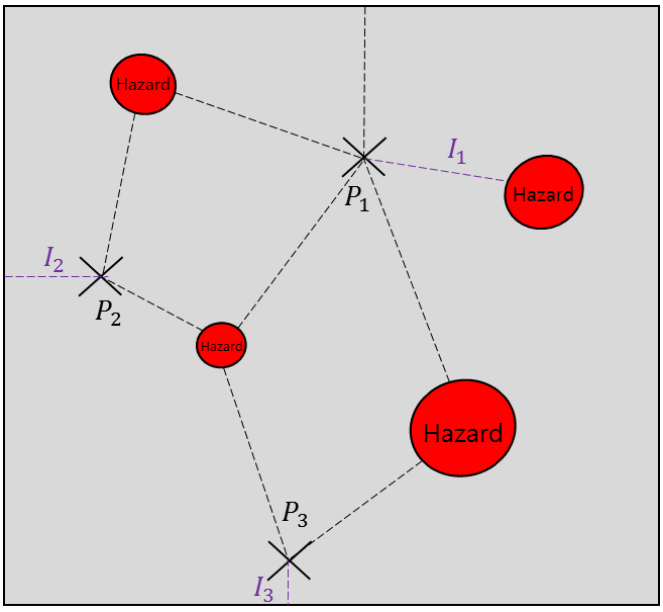

Figure 2.5 Distance from points to the nearest hazard

the maximum tolerance. For instance, as shown in Figure 2.5, the cost on P_1 has the smallest value since distance to the nearest hazard I_1 of P_1 is the biggest among I_1, I_2 and I_3. In this manner, two hazard cost maps based on relative distance to slants and rocks respectively is acquired by calculating cost according to all the point on the landing area. We define hazard cost map related to relative distance to slant is Distance To Nearest Slant (DTNS) cost map and that related to relative distance to rock is Distance To Nearest Rock (DTNR) cost map. The edge of each cost maps are also hazardous area and cost is set to one because there is no clear information whether slants or rocks exist outside the map or not.

2.6 Hazard Cost Integration

Terrain parameters and distance based hazard costs $\mathbf{C}_k$ can be integrated to one hazard cost map $\mathbf{C}_{\text{integrated}}$. In the integrated cost map, the point with the minimum cost is selected as the best safe landing point. The integration is performed by weighted sum of hazard cost maps based on terrain parameters, DTNR and DTNS. In this case, the weights called ‘MapCost’ according to each cost map is calculated from sum of total cost of each hazard cost map [8].

$$\text{MapCost}_k = \sum_{i=1}^{n}\sum_{j=1}^{m}\mathbf{C}_{k,ij} \quad \begin{matrix} i,j\text{: pixel index} \\ k\text{ : hazard cost maps based on terrain parameters, DTNR and DTNS} \end{matrix} \tag{16}$$

$$w_k = \frac{\text{MapCost}_k}{\sum_{k=1:3}\text{MapCost}_k} \tag{17}$$

$$\mathbf{C}_{\text{Integrated}} = \sum_{k=1:3} w_k \mathbf{C}_k \tag{18}$$

This is a reasonable approach because the sum of total cost can be a good information which helps to adaptively reflect the local characteristics of the lunar terrain. For instance, if the total cost of the DTNS cost map is bigger than that of the DTNR cost map, the terrain has a lot of slants but it is not relatively rough.

Chapter 3

Performance Analysis of Landing Point Designation

3.1 Lidar Model

The Lidar measurement for the HDA simulation is generated by a Lidar model. In this simulation, the 2-axis gimbaled scanning model which is divided into scanning and range model is applied[6]. The scanning model has a laser angle coordinate which is obtained by discretizing Lidar's field of view according to scanning resolution. In this

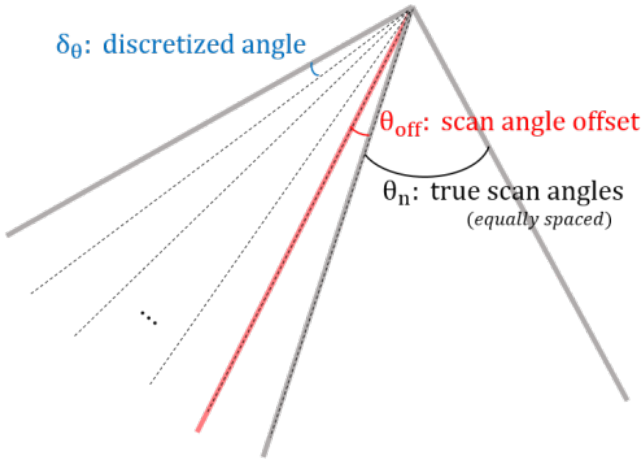

Figure 3.1 Scanning model

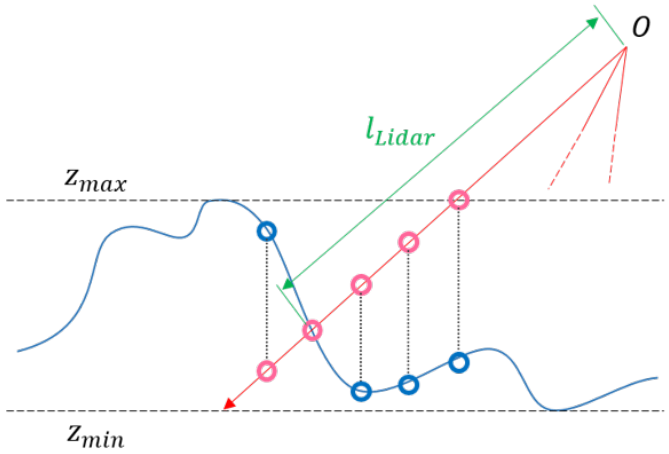

Figure 3.2 Range model

case, each angle has an offset error of Gaussian white noise.

$$\mathbf{r}(t) = [r_x(t), r_y(t), r_z(t)] = a + \mathbf{b}t, \quad \|\mathbf{b}\| = 1 \tag{19}$$

$$\mathbf{b} = \left[x_n,\ y_n, z_n\right] = \frac{\left[L\tan\theta_n,\ L\tan\phi_n,\ L\right]}{\sqrt{(L\tan\theta_n)^2 + (L\tan\phi_n)^2 + L^2}} \tag{20}$$

The laser vectors are then calculated as where θ and ϕ are the angles of horizontal and vertical direction respectively as illustrated in Figure 3.1. The discretized angular coordinate determines direction of each laser vector. The scan angle offset is regarded as white noise of small angle position defined by dividing a scan angle. In the range model, the distance between the origin of Lidar coordinate and the point laser vector is reflected. In order to find the reflection point, the ray tracing

technique increases vector length from the point of the maximum elevation to that of the minimum elevation, and compares z position of the vector to reference elevation on the same horizontal point. The transition point that reference elevation is bigger than z position of laser vector is determined as the reflection point of the laser. The range measurement L is generated by the distance between the transition point and Lidar. In this simulation, the HDA algorithm was performed by the measurement.

3.2 Simulation of Safe Landing Point Designation with respect to Lunar Terrain

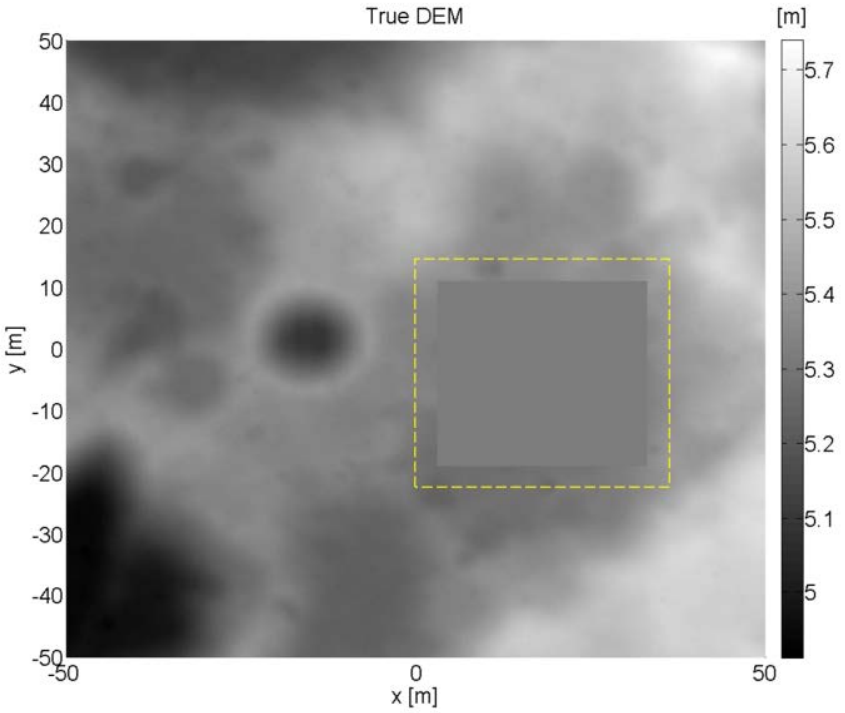

Figure 3.3 Reference lunar DEM of landing area with an arbitrary safe zone(yellow box)

Monte Carlo simulation has been conducted integrating the terrain parameters, DTNR and DTNS cost maps in four combinations in order to designate the best safe landing site(LS). Modified LOLA data of LRO that horizontal and vertical dimension was scaled down was used and arbitrary safe zone which is gentle and smooth without any slant or rocks on the middle and right of the reference DEM(yellow box) as illustrated in Figure 3.3. The simulation condition is shown in Table 3.1.

Table 3.1 HDA simulation condition

Parameter	**Value**
Reference DEM: size	100m
Reference DEM: resolution	0.1m
Altitude	500m
Lidar: FOV	10°
Lidar: resolution	100
Lidar: range error	0.02m(1-σ)
Lidar: mirror angle error	None
Lander footprint	5m
Probability at least a plane without outlier(P)	0.99
Rock distribution(o)	0.1
Tolerance: slope	5°
Tolerance: roughness	0.3m

3.2.1 Lidar Measurement Generation

The 100 by 100 Lidar measurement was generated with respect to the reference DEM as shown in Figure 3.4. The horizontal size with 10° of FOV is 87.5m at 500m high by the measurement.

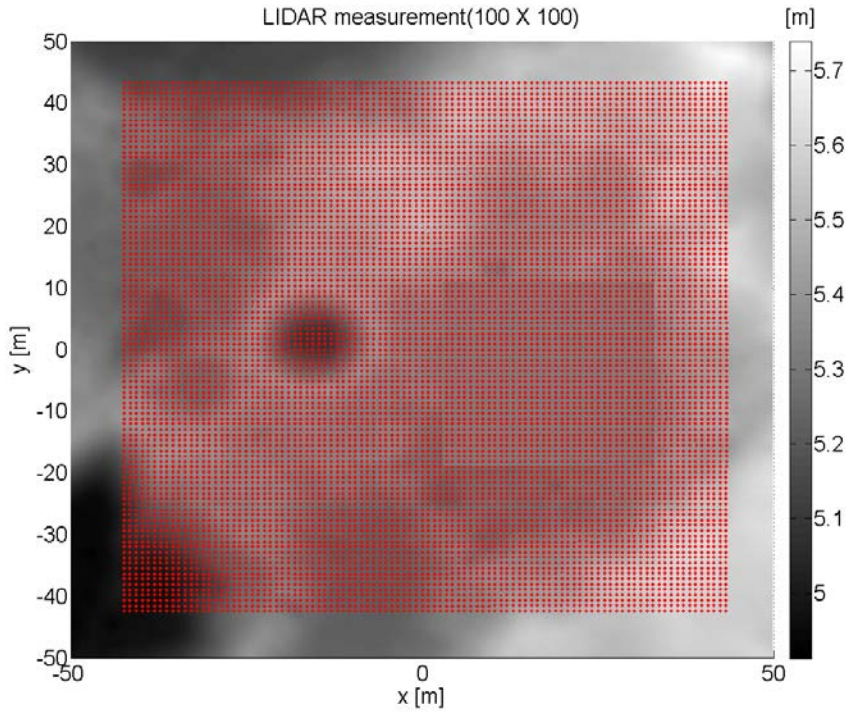

Figure 3.4 Lidar measurement with respect to the reference terrain

3.2.2 Uniform DEM Generation

The Lidar measurement is not deployed regularly because it is scanning Lidar which defines angle vectors with even angular space. However, this makes the measurements

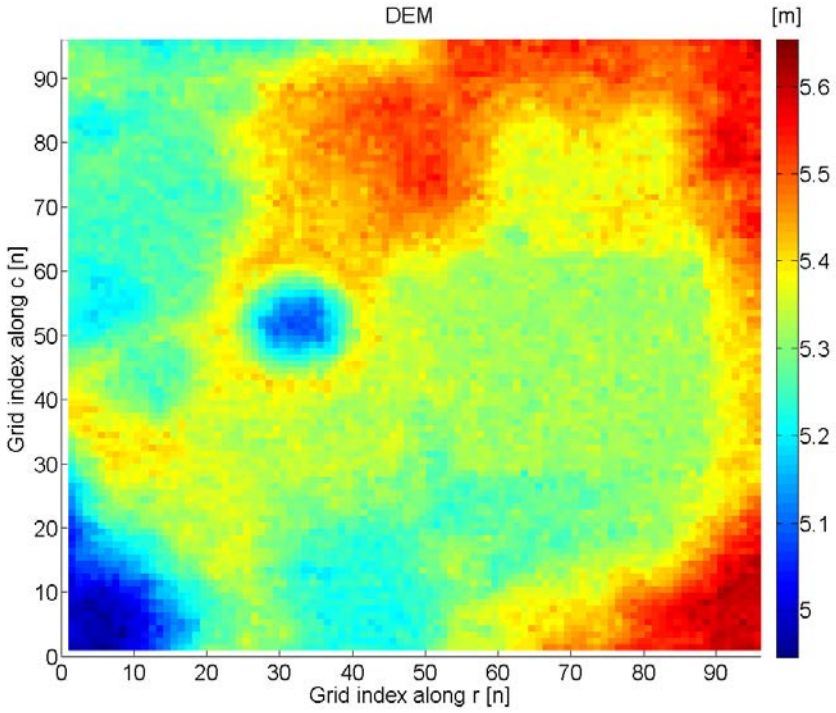

Figure 3.5 Lunar terrain DEM generated by regridding

on the point of laser reflection located irregularly. Besides, the terrain characteristics and measurement noise contribute to the unevenness. Using the data directly to the HDA algorithm is not efficient. Thus, the regridding technique reconstructs DEM by uniformly mapping the measurement on the equally spaced grid. The space between a grid node and another is defined by GSD as shown in Chapter 2. The refined DEM from the Lidar measurement was generated as shown in Figure 3.5.

3.2.3 Terrain Parameter and Integrated Hazard Cost Calculation

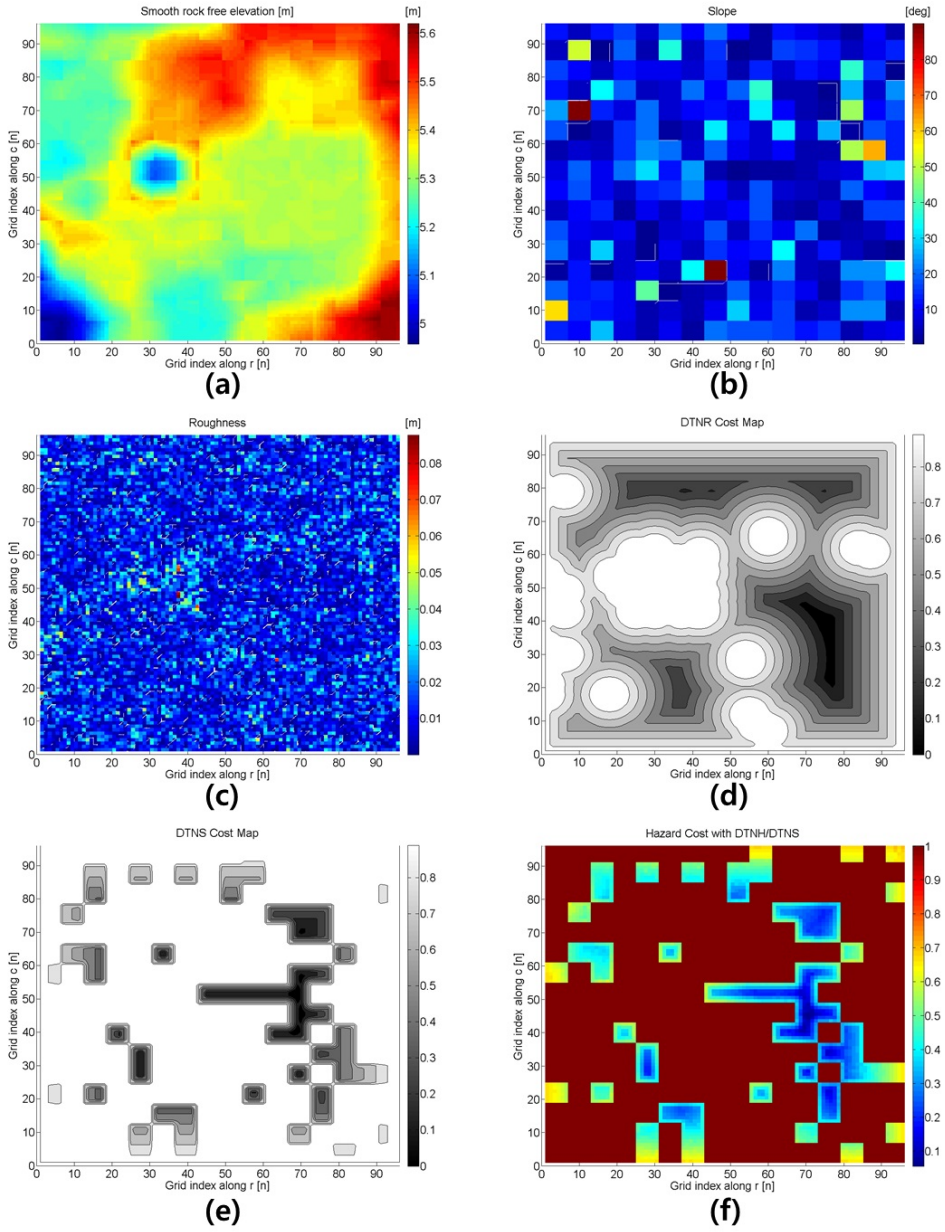

Figure 3.6 One-time safe landing simulation result; DEM of approximated plane(a), slope(b), roughness(c), DTNR cost map(d), DTNS cost map(e), hazard cost map(f)

A integrated hazard cost map(f) was generated by calculating DEM on the uniform grid(a), slope(b), roughness(c), DTNR(d) and DTNS(e) cost maps as shown in Figure 3.6. The DEM has elevation between 5 to 6.5m. The smooth outlier-free elevation map was generated by approximating genuine terrain to the combination of unit planes. The slope and roughness of the maps about them are distributed from 0 to 90deg and from 0 to 0.22m respectively. The distance-to hazard-based and integrated cost maps have the normalized cost from 0 to 1. The final results of landing point designation are compared and analyzed as below. Accordingly, the safest landing target with minimum hazard cost is designated in the safe zone by the integrated hazard cost map as illustrated in Figure 3.7.

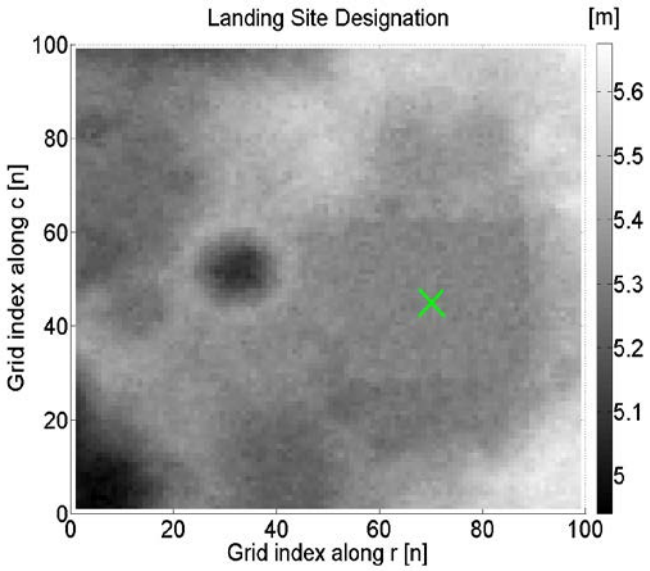

Figure 3.7 Landing point designation result by the integrated hazard cost map

3.3 Performance Analysis of Landing Target Selection

HDA simulation results are analyzed according to various combination of hazard cost maps and terrain condition. There are three kinds of integration strategies: HDA only with terrain parameters(LS), HDA by the combination of the parameters and the DTNR cost map(LS with DTNR), HDA with the terrain parameters and the DTNS(LS with DTNS), and HDA by the integration of all the hazard cost maps(LS with DTNR/DTNS). The performance of the strategies are compared each other according to terrain conditions of high roughness and the slope. The terrain condition can be confirmed through the terrain parameter estimates as shown in Table 3.3.

3.3.1 Landing Point Designation with respect to a Terrain with Extreme Slope Change

In this simulation, the DEM of simple terrain with extreme change of the slope(steep train) was utilized. Rock-shaped hazards are regularly distributed on the plat surface and arbitrary safe area(black flat surface) is predefined as shown in Figure 3.8. As a result of the simulation about this terrain, most landing targets are successfully designated in the safe zone regardless of any designation strategy. However, root mean square values of position error between the selected landing point and the center of the safe zone in Table 3.4 shows that the performance of the HDA strategy with DTNS is the best while that of the strategy with DTNR is poor since the roughness estimate is

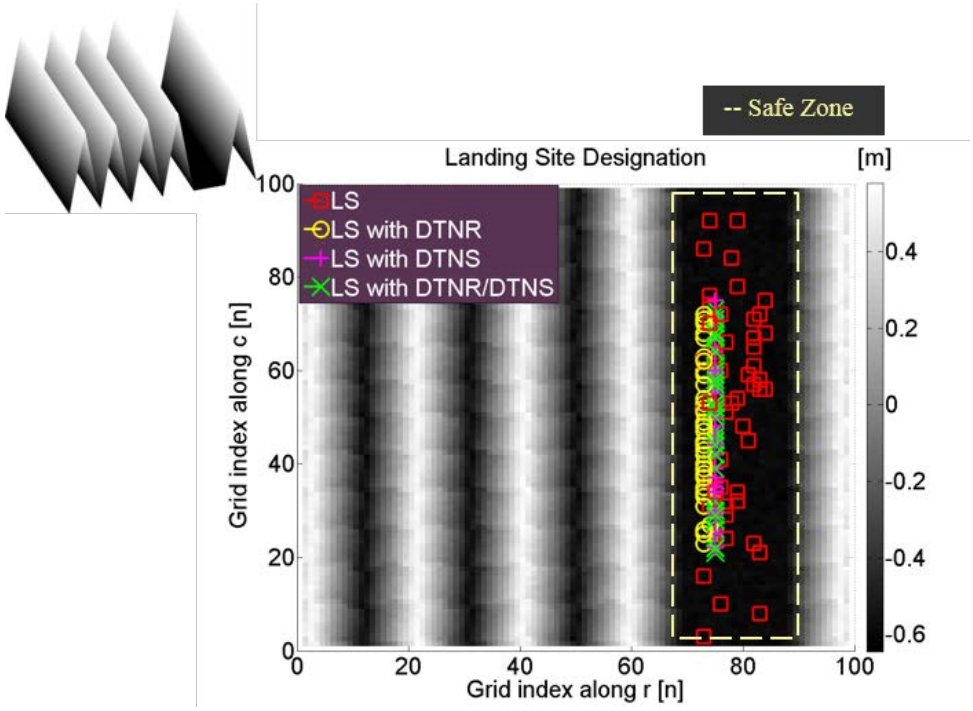

Figure 3.8 Monte Carlo simulation of landing point designation according to a terrain with extreme slope change

easily affected by measurement noise resulting in rock detection error.

3.3.2 Landing Point Designation with respect to a Rough Terrain

The simulation has been conducted according to a rough terrain without the slants as illustrated in Figure 3.9. The simulation result shows that the HDA strategy with DTNR is the best since the measurement to noise ratio is very high and rocks can be accurately detected whereas the HDA performance with DTNS is poor because the

slope estimate is likely to be influenced by the noise and the rocks. Thus, the slope has large estimation error resulting in big rms of position from the landing target to the center of the safe zone as shown in Table 3.4.

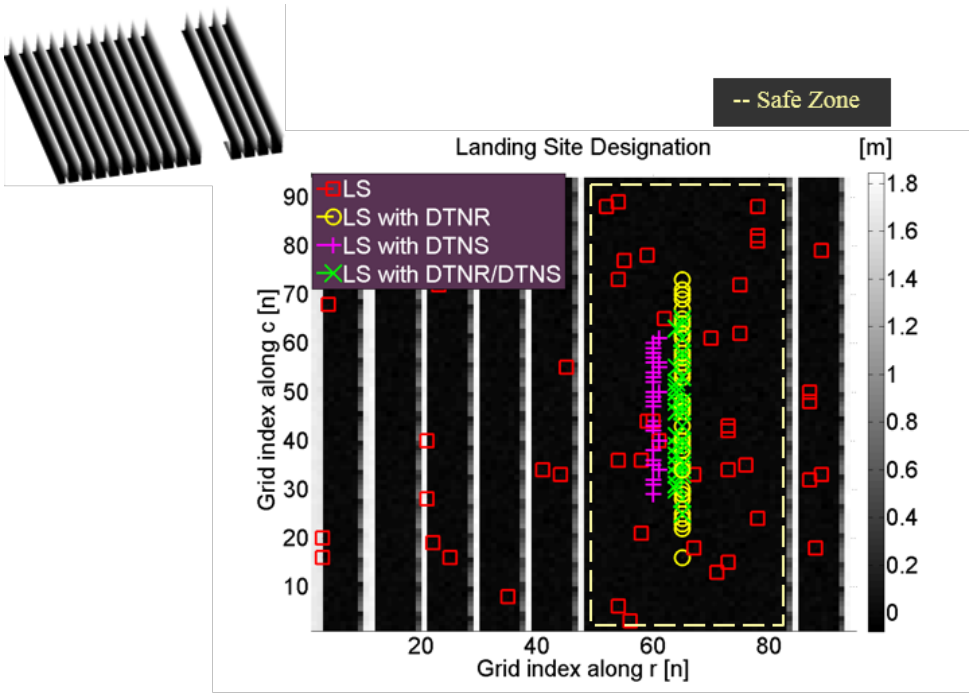

Figure 3.9 Monte Carlo simulation of landing point designation according to a rough terrain

3.3.3 Landing Point Designation with respect to Lunar Terrain

In this simulation, three lunar DEMs with different topological characteristics were used for the comparison of HDA performance on the lunar surface. The simulation results according to the terrain with extreme slope change and that with huge roughness is illustrated in Figure 3.10, 3.11. Moreover, the HDA simulation was also conducted with the smooth lunar surface with very low slope and roughness as shown in Figure 3.12.

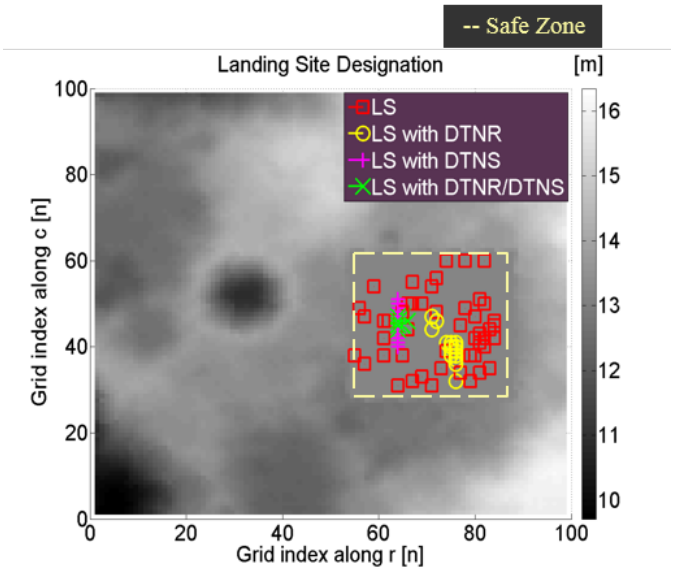

Figure 3.10 Monte Carlo simulation of landing point designation according to steep lunar terrain with extreme slope change

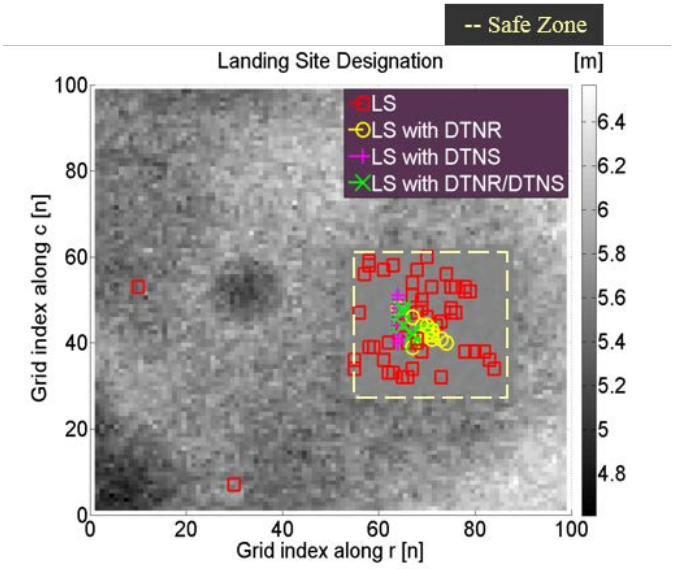

Figure 3.11 Monte Carlo simulation of landing point designation according to rough lunar terrain

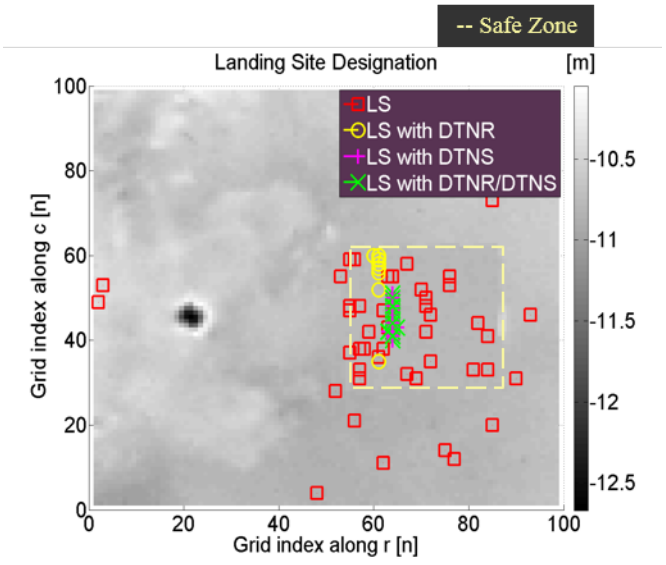

Figure 3.12 Monte Carlo simulation of landing point designation according to smooth lunar terrain with low slope and roughness

3.3.4 Comparison of the HDA Performance according to Terrain Condition

The HDA simulation has been conducted according to various terrain conditions reflected in two simplified DEMs and lunar DEMs characterized by three different terrain conditions. First of all, The Monte Carlo simulation results with respect to the terrain maps with extreme slope change or the severely rough terrain shows good safe landing probability which is defined the probability of landing point designation on the predefined safe zone without any consideration of hazard cost based on distance to hazard as shown in Figure 3.10, 3.11. However, In the case of the relatively smooth and gentle terrain, the safe landing probability of HDA only with the terrain parameters is even very low since the noise and the tolerance level is similar to the terrain parameter estimates which are vulnerable to the noise.

HDA with at least one hazard cost between DTNR or DTNS shows nearly 100% of safe landing probability as shown in Table 3.3. This seems that HDA only with one of two distance-to-hazard-based hazard cost guarantees good safe landing performance, but it does not. The HDA performance can be better obviously compared with root mean square values of position error between the selected landing point and the center of the safe zone in Table 3.4.

In the case of steep terrain with extreme slope change, the HDA strategy with DTNS shows the best safe landing performance with the smallest rms value. The HDA

performance with DTNR is worse because the roughness estimate is close to the range noise and easily affected the noise resulting in rock detection error.

Meanwhile, in the case of rough terrain, the performance of HDA with DTNR is the best since the slope estimate is likely to be influenced by the range measurement error. If DTNR is not considered, the designated landing target can be located close to rocks since distance to rocks were not considered in the hazard cost calculation.

In the case of HDA with both DTNS and DTNR, it shows the best performance regardless of the terrain condition considering the distance to the slants and rocks and designating the farthest landing point from them.

Table 3.2 Mean roughness and slope with respect to simple terrain and lunar terrain

Terrain parameter / Terrain condition	Roughness(m)	Slope(deg)
Steep	0.04	43.1
Rough	0.22	17.4
Lunar(steep)	0.05	36.1
Lunar (rough)	0.08	14.8
Lunar(smooth)	0.02	8.5

Table 3.3 Safe landing probability of target designation in the safe zone with respect to four hazard avoidance strategies

[%]

Strategy / Terrain condition	LS only with Terrain Parameter	LS With DTNR	LS With DTNS	LS With DTNR/DTNS
Steep	88	100	100	100
Rough	98	100	100	100
Lunar(steep)	92	98	100	100
Lunar (rough)	92	100	100	100
Lunar(smooth)	42	100	100	100

Table 3.4 RMSE of position between the center of safe zone and selected landing target

[m]

Strategy / Terrain condition	LS	LS With DTNR	LS With DTNS	LS With DTNR/DTNS
Steep	5.3	3.8	0.9	1.7
Rough	29.6	0.3	4.9	0.4
Lunar(steep)	15.5	9.9	5.4	4.1
Lunar (rough)	14.5	4.1	5.2	4.1
Lunar(smooth)	32.1	15.4	5.4	5.4

3.4 Summary

The simulation results assert that the landing target designation only with terrain parameters or one of the two distance-to-hazard-based-cost is vulnerable to the sensor measurement noise and terrain condition losing consistency. To improving safe landing performance, hazard cost map based on distance to the nearest rocks and the slants should be applied simultaneously to the hazard cost of terrain parameters in order to prevent the landing target from being designated near any kind of hazard. In this case, the distance-to-slant-based hazard cost has more effect on the degradation of the HDA performance than hazard cost based on distance to the nearest rocks since the slope is estimated by the pixels as big as the landers footprint.

Chapter 4

HDA Experiment Using Quadrotor Equipped with TOF Camera

4.1 Introduction

A quadrotor is an unmanned aerial vehicle (UAV) flying by four rotors. This flying robot is able to perform precise vertical and directional flight. It has been developed in

Figure 4.1 Indoor HDA experiment with quadrotor

a wide variety of research and industrial fields in various types and size. Especially, the quadrotor can be made small and light that enables indoor autopilot research. Thus, it provides a good HDA experiment environment to imitate actual lunar landing scenario and can be use to confirm feasibility of the HDA technique.

4.2 Experiment Environment

In this experiment, a simplified terrain model imitating lunar surface was used. The model has rocks in various size, and a slant without any rocks exists in 1/3 under the terrain model as shown in Figure 4.2.

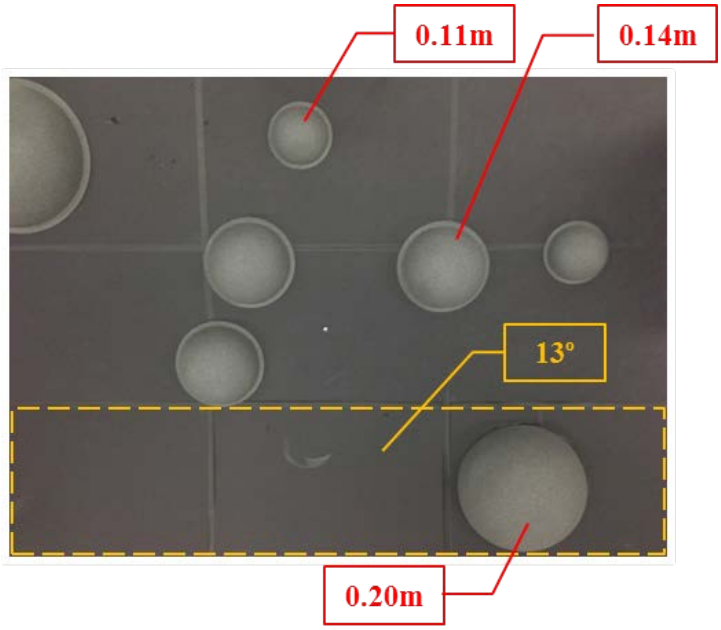

Figure 4.2 Lunar surface model for HDA experiment based on TOF camera

The model was utilized to verify the problem occurring if the one of the distance-based hazard cost map had only been considered and to analyze the change of performance with both DTNR and DTNS cost maps.

In order to acquire the range measurement with respect to the lunar surface model, SR4k Time Of Flight (TOF) camera of Heptagon enterprise system which is one of the sensors providing three-dimensional point cloud like a flash Lidar was used. Even though the depth-camera emitting IR instead of laser, it counts the time of flying light emitted, reflected and returning to a CCD sensor of the camera similar to flash Lidar[9]. This camera is an appropriate sensor which is much lighter and affordable for experiment and proof of the HDA performance than flash Lidar used for the actual lunar lander. This acquires range measurements, and they are transmited to the GCS by a C++ program based on SR4k library.

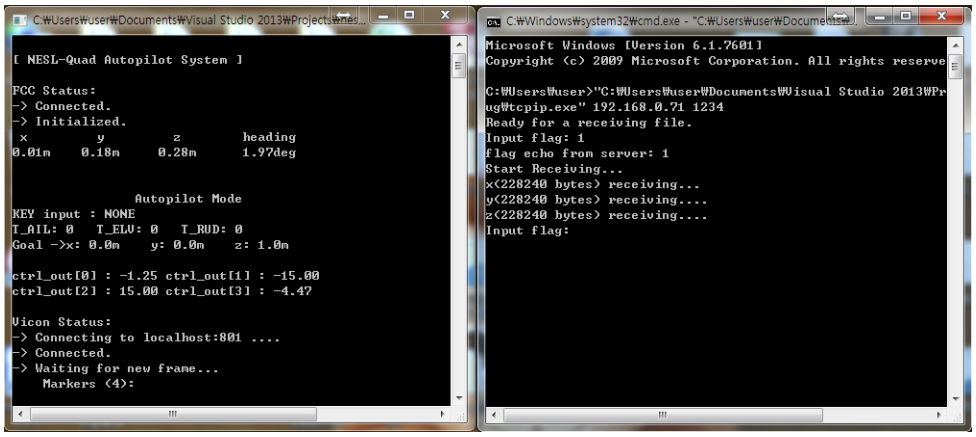

Figure 4.3 Ground control system for quadrotor and TOF camera control: quadrotor autopilot software(left) and TOF camera measurement acquisition software(right)

In this case, a Gaussian filter was applied to make the signal to noise ratio (SNR) similar to that of the range measurement of the flash Lidar.

This camera and StickPC which is a light weight micro PC with Ubuntu are loaded on a small quadrotor and the StickPC transmits the measurement to Ground Control System (GCS) through TCP/IP wireless network.

DJI's NAZA flight control computer (FCC) including inertial measurement unit(IMU) and hovering algorithm which provides basic horizontal stability. The FCC basically receives pulse width modulation (PWM) of the command signals from the RC transmitter and maneuvers following it.

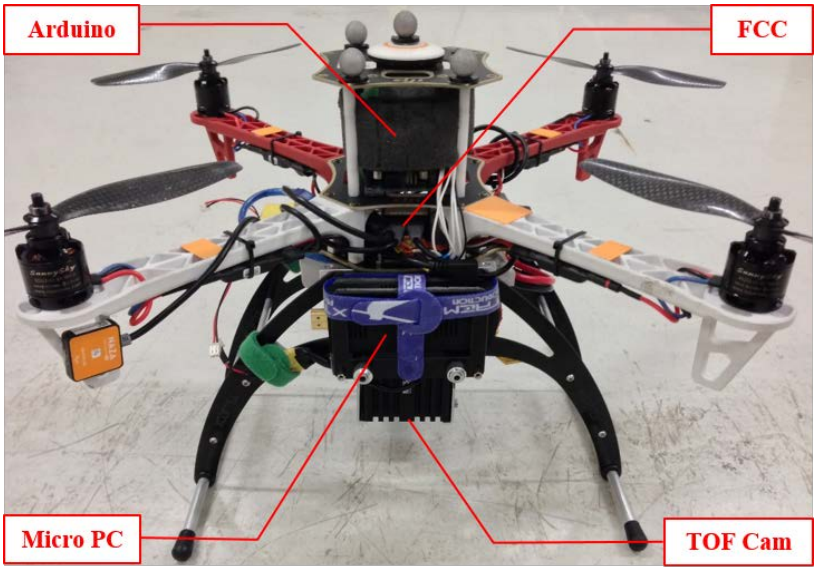

Figure 4.4 Quadrotor equipped with TOF Camera

The PWM signals same as that from the transmitter were generated on 12-bit PWM generator connected to Arduino Uno which is an embedded microcontroller based on ATmega328 since the Arduino is able to generate only 3 Timer counter while at least 5 PWM signals are needed to control the NAZA FCC.

The GCS receives the VICON position data which precisely tracks small IR-reflective markers on the quadrotor, and calculates the quadrotor's position and attitude.

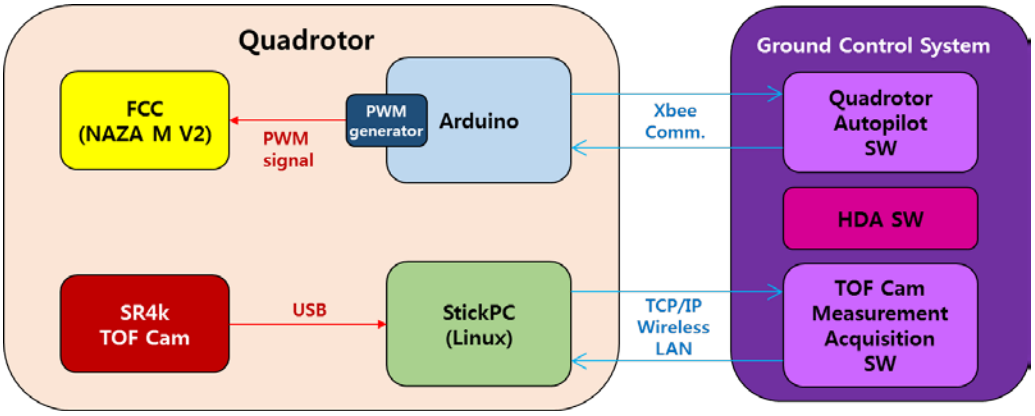

Figure 4.5 Scheme of quadrotor-based HDA experiment system

The C++ quadrotor Autopilot Software based on real-time Datastream SDK of VICON generates manual and autopilot flight command and transmits them through Xbee which is a short-range wireless serial communication module. The Arduino embedded in the quadrotor receives the command and controls it following the PWM signal generated based on the command from the GCS.

4.3 HDA Experiment Based on Quadrotor Autopilot System with TOF Camera

The entire quadrotor system for the HDA experiment is composed as shown in Figure 3.6. The quadrotor autopilot software calculates the quadrotors position and heading data using the VICON position measurement. The VICON measures position

of markers attached onto the quadrotor. The position of the quadrotor is calculated by the average position of the attached markers. A heading vector is defined by the two marker's position and heading angle is acquired This vector is defined by the projection of the vector on the horizontal plane of the VICON reference coordinate system and the heading angle can be obtained by calculating the angle between the vector and y-axis of the reference frame using inner product of the two. The autopilot program gets the position and heading attitude and generates PID control commands using them in order to control the quadrotor flying toward desired position. The control output data is sent to the quadrotor through Xbee communication. The Arduino on the quadrotor generates motor driving signal based on the command.

The TOF camera measurement acquisition software runs to get the three-dimensional range measurement from the TOF camera. This program on the StickPC save the measurement and sends it to the GCS through the TCP/IP wireless communication. The size of the data is approximately 700kB and it takes around 15 second to transmit all the three axis position data of the point cloud.

The HDA software runs in MATLAB and designates the best safe landing point in the landing area using the range measurement. Once the best landing target is designated as a result of the HDA algorithm, the position on the Hazard cost map is

converted to a command for actual position control. Finally it lands on the selected point automatically. The experiment condition is stated in Table 4.1

Table 4.1 Experiment condition

Parameter	**Value**
Reference DEM: size	2.75x2.13m
Rock size: big	0.20m
Rock size: medium	0.14m
Rock size: small	0.11m
Slant slope	13°
Altitude	2m
TOF cam: FOV	69°x56°
TOF cam: resolution	176(h)x144(v)
TOF cam: range error*	0.01m(1-σ)
Lander footprint	0.2m
Tolerance: slope	10°
Tolerance: roughness	0.02m

*Guassian filter applied

4.4 Experiment Result of Quadrotor Safe Landing Based on HDA

The experiment result using the camera measurement shows that the performance of landing site designation only with terrain parameters is worst like simulation result as illustrated in Figure 4.6. The result of the HDA with DTNR cost map also shows landing target on or near hazards because of the range measurement error. It causes the slope estimation error interfering with the detection of the slants. In this case, if rocks

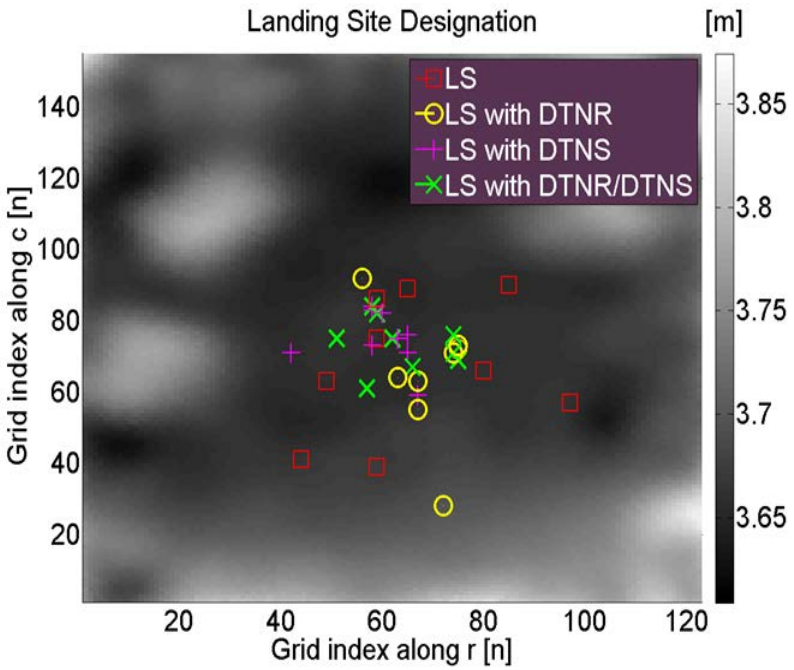

Figure 4.6 HDA Landing Experiment Result

are not detected, the pixels in the area have low hazard cost since distance to the slants was ignored. Thus, there is a possibility that landing points are selected among them if the slants are smooth without any rocks. In the case of the designation with DTNR and DTNS cost map, the safest landing points which are as far from both the slants and rocks as possible, and have low hazard cost can be selected.

4.5 Summary

The experiment of the HDA technique using the quadrotor equipped with the TOF camera was conducted. This camera measured the three-dimensional vertical range from it to the lunar surface model. The model has rocks and the slants in various size. The quadrotor hovered above the terrain and transmitted range data through the wireless network to the GCS for the HDA operation and the designation of the best safe landing point. The HDA algorithm found the safe point and the quadrotor finally landed on the selected landing target. The experiment results show that the integration of both DTNR and DTNS cost map resulted in the designation of the safest landing point.

Chapter 5

Conclusions

A HDA system is necessary to precisely detect hazards such as craters, rocks and slants which pose a threat to the lunar lander and avoid them. In this thesis, the research sheds light on the limitation of safe landing point designation only with the terrain parameters: the slope and roughness and insists of the importance of hazard cost maps which are called DTNR and DTNS cost map based on relative distance to the slants and rocks defined by the parameters in order to overcome it. What is more, this thesis asserts a significance of the integration considering both DTNR and DTNS with terrain parameters and shows it relating to the characteristics of terrain by simulation and experiment.

The simulation results showed that precise and consistent landing point selection only with the hazard cost from terrain parameters impossible and the performance can be improved by combining it with DTNR or DTNS cost maps. However, the integration with DTNR or DTNS respectively still results in landing point designation near or on the hazards. Accordingly, the integration of hazard cost maps with both DTNR and DTNS cost maps shows the best performance of safe landing target selection as far from all the hazards as possible.

The experiment using a quadrotor autopilot system equipped with TOF camera shows the feasibility of the HDA technique based on hazard cost map combined with the distance-to-hazard-based hazard cost maps.

Bibliography

[1] Epp, Chirold D., and Thomas B. Smith. "Autonomous Precision Landing and Hazard Detection and Avoidance Technology (ALHAT)," *IEEE Aerospace Conference*, Big Sky, Montana, 3 – 10 March 2007.

[2] Brady, Tye, and Stephen Paschall. "The challenge of safe lunar landing," *IEEE Aerospace Conference*, Big Sky, Montana, 6 – 13 March 2010.

[3] Shankar, Uday J., et al. "Lunar Terrain Surface Modeling for the ALHAT Program," *IEEE Aerospace Conference*, Big Sky, Montana, 1 – 8 March 2008.

[4] Serrano, Navid, et al. "A novel tiered sensor fusion approach for terrain characterization and safe landing assessment," *IEEE Aerospace Conference*, Big Sky, Montana, 4 – 11 March 2006.

[5] Huertas, Andres, Yang Cheng, and Richard Madison. "Passive imaging based multi-cue hazard detection for spacecraft safe landing," *IEEE Aerospace Conference*, Big Sky, Montana, 4 – 11 March 2006.

[6] Johnson, Andrew E., et al. "Lidar-Based Hazard Avoidance for Safe Landing on Mars," *Journal of Guidance, Control and Dynamics*, Vol. 25, No. 6, 2002, pp. 1091~1099.

[7] Johnson, Andrew E., et al. "Analysis of On-Board Hazard Detection and Avoidance for Safe Lunar Landing," *IEEE Aerospace Conference*, Big Sky, Montana, 1 – 8 March 2008.

[8] Cohanim, Babak E., and Brian K. Collins. "Landing Point Designation Algorithm for Lunar Landing," *Journal of Spacecraft and Rockets*, Vol. 46, No.4, 2009,

pp.858-864.

[9] J. de Lafontaine, D. Neveu and K. Lebel, “Autonomous planetary landing using a LIDAR sensor: the closed-loop system,” *In Proceedings of 6th International ESA Conference on GNC Systems*, Loutraki, Greece, 17 – 20 October 2005.

[10] Gribbon, K. T. and Bailey, D. G., "A Novel Approach to Real-time Bilinear Interpolation," *Second IEEE International Workshop on Electronic Design, Test and Applications*, Perth, Australia, 28 – 30 January 2004.

[11] T. Masuda, K. Sakaue, and N. Yokoya. “Registration and integration of multiple range images for 3-d model construction,” *In Proceedings of the 1996 International Conference on Pattern Recognition*, Washington, DC, USA, 25 – 29 August 1996.

[12] Duda R., and Hart P., *Pattern Classification and Scene Analysis, Wiley-Interscience*, New York, 1973, pp. 116 – 119

국문초록

달착륙선의 라이다 기반 위험회피 착륙시스템은 기본적으로 착륙지형 파라미터인 경사와 험준도로 위험도를 계산하고 위험도가 최소값을 갖는 점을 안전한 착륙 지점으로 선정한다. 이때, 경사와 험준도만을 고려할 경우 라이다 측정오차에 의해 착륙지가 위험요소 근처로 선정될 수 있으며 이는 착륙선에 위협적이다. 이러한 문제를 해결하고 최대한 안전한 착륙지점을 선정하기 위하여 위험상대거리 기반의 위험도를 기존의 지형파리미터 기반의 위험도와 함께 고려하여야 한다. 이 때 위험상대거리 기반 위험도와 지형 특성간의 관계가 위험회피 착륙기법 성능에 미치는 영향에 대한 면밀한 분석이 필요하다. 논문에서는 경사와 험준도 각각에 대한 위험상대거리 기반 위험도가 지형 특성에 따라 착륙지 선정결과에 미치는 영향을 분석하였다. 또한 시뮬레이션과 삼차원 뎁스 카메라를 장착한 쿼드로터 기반 실험을 통해 두 가지 위험상대거리를 동시에 고려하였을 때 가장 좋은 위험회피 착륙 성능을 나타냄을 확인하였다.

주요어: 달 착륙, 위험회피착륙, 라이다, 뎁스카메라, 쿼드로터

이 름: 이 충 민

학 번: 2014-20663